Aerotecnica Missili & Spazio (2022) 101:371–385
https://doi.org/10.1007/s42496-022-00129-2

ORIGINAL ARTICLE

Analysis of an Acoustic Monopole Source in a Closed Cavity via CUF Finite Elements

M. C. Moruzzi[1] · **M. Cinefra**[2] · **S. Bagassi**[1]

Received: 8 December 2021 / Revised: 21 July 2022 / Accepted: 23 July 2022 / Published online: 9 August 2022

Abstract
The noise generated by aircraft is an important issue, which affects the external environment and the passenger's comfort. The researches about new acoustic solutions often lead to the exploitation of innovative materials, as visco-elastic panels or acoustic metamaterials, in order to rather obtain better acoustic properties than conventional materials, in particular at low frequency. Although, there is a lack of reliable tools able to describe the complex kinematic behaviour of these new materials at low frequency. A new strong formulation, the Carrera Unified Formulation (CUF) based on the Finite Element Method (FEM), enables a wide class of refined shell models, which is able to reproduce the frequency dependent dynamic response of complex multi-layered plates. This formulation, fully developed inside the MUL2 software, is applied to vibro-acoustic analyses too, so the need to integrate new sources and boundary conditions in the software, that are essential to model the acoustic problem. A simple and powerful source is the monopole: a pulsating sphere. This source can be a first try to model the complex sources that affect the noise inside the aircraft, as the engine or the internal sources. Moreover, monopoles are widely used to estimate the transmission loss. Hence, the reason for this work: the creation inside MUL2 of a monopole boundary condition and its validation, comparing the results with those of a well-known FEM based commercial software for vibro-acoustic analyses, Actran.

Keywords Acoustics · Carrera's Unified Formulation · Spherical source · Closed cavity · Finite Element Method

1 Introduction

Aircraft generate noise, which can affect the environment, as the people who live and work near the airport, as well as the wildlife [1, 2]. Moreover, noise can follow structure-born path inside the aircraft, generating vibrations, which can damage the structure, and lowering the comfort level inside the passenger cabin [3]. Therefore, in last 30 years a great interest in noise and vibrations reduction has led to several researches, regarding both the understanding of the physical phenomena behind the noise generation and the search for solutions to reduce it [4, 5].

An important link between the understanding of the noise generation process and the search for an optimal noise reduction solution is the chance to perform accurate on-field and numerical tests. The understanding of the noise generation phenomena represent an essential tool to study the problem, but they are limited by physical and economic constraints, in particular regarding the design and development of acoustic solutions in the complex aircraft environment. The optimization of the noise reduction solutions allows to study the aircraft acoustic behaviour and develop noise abatement solution with a greater flexibility than on-field tests. Although, they can not always fully understand the complex acoustic behaviour of the analysed components, in particular when there is coupling between the components, as those between the vibrations of the structure and the fluid pressure or those between several structural elements of the aircraft.

The aircraft noise problem involves several disciplines and can be studied using various approaches. The vibro-acoustics describes the interaction between the structural displacements and the pressure in the fluid, the so called vibro-acoustic coupling. The acoustic behaviour of the aircraft structure is investigated in order to understand the

✉ M. C. Moruzzi
martinocarlo.moruzz2@unibo.it

[1] Department of Industrial Engineering, Università di Bologna, Via Fontanelle, 40, 47121 Forlì, Italy

[2] Department of Mechanical, Mathematics and Management, Politecnico di Bari, Via Orabona, 4, 70125 Bari, Italy

contribute of each structural component to the noise generation process [6, 7]. Moreover, several solutions for noise reduction are based on the absorption of the vibrations [8, 9], so they must be investigated in the vibro-acoustic field. Visco-elastic materials, as those placed in sandwich plate, are a common and powerful solution to reduce noise [10, 11], absorbing the vibrations around an acoustic source or shielding a defined area, as the passenger cabin, from the incoming acoustic waves.

Numerical tools, able to predict the vibro-acoustic problem's frequency dependence response, are usually based on the finite element method (FEM) for low frequency [12] and on statistical energy analysis (SEA) for high frequency [13]. Hybrid methods can be applied for mid frequency range [14]. The low frequency problem is well known and described [15]. Although, there is a lack of numerical reliable tools for innovative materials, that are able to describe the complex kinematic behaviour of visco-elastic and composite materials, avoiding an important increase in the computational cost of the numerical analysis. Indeed, researchers usually study this kind of material in a numerical environment through three dimensional models, because two-dimensional ones are not able to correctly predict the dynamic response of the structure [16, 17]. In order to correctly reproduce the complex kinematic behaviour of these innovative materials a powerful notation is exploited: the Carrera's Unified Formulation (CUF) [18]. This formulation enables a wide class of refined plate theories through the Layer Wise (LW) approach [19]. The software MUL2[1] was developed to exploits this formulation for static and dynamic structural analyses. However, the CUF formulation and the LW structural models are useful in the acoustics too, both to reduce the computational cost and to have an accurate description of the structural displacements. So MUL2 was expanded to work in the vibro-acoustic field, with the introduction of the acoustic model and of the resultant coupling. The reliability of the software (and of its numerical model) and its advantages have been already studied and estimated in [20], where the authors compare the MUL2's results with those obtained by analyses based on an Equivalent Single Layer (ESL) model for a cavity-plate coupled system.

The acoustic sources have an important role in the noise prediction analyses. Although, the aircraft noise sources are complex entities to be modelled and not always completely understood [21]. They require a high degree of fidelity and a high amount of information, that are not always available, in particular in the preliminary design stage. For these reasons in the complex FEM model sources are simplified, splitting the problem in a first one about the definition of the source and a second one on the study of the vibro-acoustic behaviour of the system. In the work by Moruzzi et al. [22] the influence on the acoustic field generated by the propellers is simplified with a diffuse pressure field on the aircraft fuselage external panels. This pressure field was previously calculated through an aero-acoustic analysis. So, the study of the source and the vibro-acoustic behaviour of the fuselage have been separated. In the work by Cinefra et al. [12], the presence of an engine, placed under the wing of a turboprop aircraft with high wing configuration, was simulated by a spherical source, a monopole, because the analysis' purpose does not require a complete description of the source.

Sources can generate vibrations, i.e. displacements, on the structure or pressure on the fluid. In MUL2, the "structural" sources, so the loads or the pressure field, are already defined as boundary conditions. Although, until now, there were not acoustic sources implemented in MUL2. A first simple source is the monopole, a spherical source which radiates sound equally well in all directions. This source can be simplified as a pulsating sphere. Even if it is a simple source, monopoles are very useful. They can be used to validate vibro-acoustic models, estimate the transmission losses of a plate and they can simulate several acoustic sources, as loudspeaker [23, 24]. Moreover, monopoles are used to simulate the engine noise as in the previous cited work by Cinefra et al. [12] or as in the work by Vieira et al. [25]. In the work by Moruzzi et al. [26], due to the lack of data, an internal source is simulated with a monopole. Finally, monopoles behaviour, at low frequency, is very similar to those of the loudspeakers.

The MUL2 validation of the new implemented source is entrusted to the commercial software Actran,[2] based on the FEM too. The software has ESL formulation for the structural elements.

2 Background Theory

2.1 Acoustic Problem

The acoustic problem in a closed cavity can be simplified as a fluid cavity domain Ω_f surrounded by rigid walls Γ_{VN} described with a Von Neumann boundary condition. The cavity fluid is defined by its density ρ_f and speed of sound c_f. The cavity is completely closed, so there are not any free surfaces and there is not the need to apply a zero pressure boundary condition (Dirichlet boundary condition).

The following hypotheses are applied to the problem:

- the fluid is homogeneous, inviscid and irrotational compressible;

[1] http://www.mul2.polito.it/.

[2] https://www.mscsoftware.com/en-uk/product/actran-vibroacoustics.

- the body forces, as the gravitational effects, are neglected.

Under these hypotheses it is possible to obtain the equations system for the fluid:

$$\begin{cases} p_{,ii} = \frac{1}{c_f^2}\ddot{p} & \text{in } \Omega_\text{f} \\ p_{,i} \cdot n_{f,i} = 0 & \text{in } \Gamma_\text{VN} \end{cases} \tag{1}$$

in which p is the fluid pressure, n_f the outward normal and dots $\ddot{}$ indicate the second derivative with respect to the time and the Einstein's summation convention is applied. The first term of the system is the wave equation, the second the Von Neumann boundary condition. At a rigid wall, the acceleration of the fluid particles must be zero and so must be the pressure gradient. Therefore, the normal velocities can be defined as follows:

$$p_{,i} \cdot n_{f,i} = -\rho_\text{f} \ddot{u}_\text{f} = 0, \tag{2}$$

where $\ddot{u}_\text{f}$ is the fluid acceleration (positive along the normal direction).

The previous strong formulation is expressed in terms of fluid pressure p. In order to obtain the variational formulation associated with the local system in Eq. 1, the test function method is applied. The weak formulation introduces arbitrary weighting functions, which represent the principal field variables that describe the evolution of the system. This weak formulation is equivalent to the Principle of Virtual Displacement (PVD) applied on the same system. The acoustic system can be written as:

$$\int_{\Omega_\text{f}} \delta p_{,i} p_{,i} \mathrm{d}V + \int_{\Omega_\text{f}} \frac{1}{c_\text{f}^2} \delta p \ddot{p} \mathrm{d}V = 0, \tag{3}$$

in which δp is the virtual pressure.

Finally, through the Fourier transform, the equation is transformed from the the time domain to the frequency one:

$$p(x_i,\ \omega) = \int_{-\infty}^{\infty} p(x_i,\ t) e^{-i\omega t} \mathrm{d}t, \tag{4}$$

where the frequency f could be written as a function of the pulsation ω, as $f = 2\pi\omega$. From the wave equation in Eq. 1 the Helmholtz equation is obtained:

$$p_{,ii} = -\frac{\omega^2}{c_f^2} p \tag{5}$$

2.2 FEM Formulation

The FE approximation is applied to the acoustic problem and the shape functions N_i are introduced to approximate the continuous pressure functions $p(x, y, z, t)$:

$$p(x, y, z, t) = N_i(x, y, z) P_i(t) \tag{6}$$

where $P_i(t)$ is nodal pressure, $i = 1; \ldots ; n^p$ and n^p is the number of nodes of the 3D fluid element.

The fluid mass matrix $\boldsymbol{Q}$ (Eq. 7) and the fluid stiffness matrix $\boldsymbol{H}$ (Eq. 9) are obtained in terms of fundamental nuclei to be coherent with the structural model based on the Carrera's Unified Formulation (CUF) [18] (fundamental nuclei are independent from the expansion order in the thickness direction for a structural element).

The mass matrix is written as follow:

$$\frac{1}{c_\text{f}^2} \int_{\Omega_\text{f}} \delta p \ddot{p} \mathrm{d}V = \delta P_j^T \boldsymbol{Q}_{ij} \ddot{P}_i, \tag{7}$$

where the fundamental nucleus expresses the inertial work

$$\boldsymbol{Q}_{ij} = \int_{\Omega_f} N_j(x, y, z) N_i(x, y, z) \mathrm{d}V. \tag{8}$$

Then, it is possible to write the stiffness matrix:

$$\int_{\Omega_f} \delta p_{,l} p_{,l} \mathrm{d}V = \delta P_j^T \boldsymbol{H}_{ij} P_i, \tag{9}$$

in which the summation index l has been introduced and the fundamental nucleus is defined as:

$$\boldsymbol{H}_{ij} = \int_{\Omega_f} N_{j,l}(x, y, z) N_{i,l}(x, y, z) \mathrm{d}V. \tag{10}$$

The problem can be expressed in a matricial form:

$$\left[\boldsymbol{Q}\right] \cdot \{\ddot{\boldsymbol{P}}\} + [\boldsymbol{H}] \cdot \{\boldsymbol{P}\} = \left\{\boldsymbol{F_p}\right\} \tag{11}$$

and in the frequency domain:

$$\left[-\omega^2 \boldsymbol{Q} + \boldsymbol{H}\right] \cdot \{\boldsymbol{P}\} = \left\{\boldsymbol{F_p}\right\} \tag{12}$$

where the last term $\boldsymbol{F_p}$ represents the external acoustic loads, as those generated by a spherical source. The fluid damping is assumed to be negligible.

2.3 Acoustic source loading

An acoustic loading is assumed to be defined by its strength, so by its volume velocity $\dot{Q}_s$ or by its power W. For a general source these parameters depend on the radiation directions, for a spherical source there is not dependency on the direction (see Sect. 3).

The acoustic load is defined in terms of Fundamental Nucleus with the Kronecker Delta δ_K (it is zero except on the position $\boldsymbol{x}_s$, where the value is unity):

$$\int_V \delta p N_j^T(x,\ y\ z)\dot{Q}_s\delta_K(\boldsymbol{x}-\boldsymbol{x}_s)dV = \delta P_j^T \boldsymbol{F}_{p_{sj}}, \tag{13}$$

where the Fundamental Nucleus is equal to:

$$\boldsymbol{F}_{p_{sj}} = \int_V N_j^T \dot{Q}_s\delta_K(\boldsymbol{x}-\boldsymbol{x}_s)\mathrm{d}V, \tag{14}$$

in which for a general source in position $\boldsymbol{x}_s$

$$\dot{Q}_\mathrm{s}\cdot e^{i\omega t} = \int_S \dot{u}_\mathrm{f}\cdot\boldsymbol{r}\mathrm{d}S, \tag{15}$$

where S is the surface on which the flux volume of velocity $\dot{u}_\mathrm{f}$ is calculated, and $\boldsymbol{r}$ is the radial vector.

3 Spherical Source

An acoustic monopole is a pulsating sphere that radiates equally in all directions [27, 28]. In order to describe the monopole pressure field, the wave equation is transformed in spherical coordinates (θ, ϕ, r). Moreover, the solution only depends on the radial terms, because the sphere pulsates equally in all directions and so the derivatives in θ and ϕ are zero:

$$\frac{\partial^2(pr)}{\partial r^2} - \frac{1}{c_\mathrm{f}^2}\frac{\partial^2(pr)}{\partial t^2} = 0, \tag{16}$$

and the general solution is:

$$p(r,t) = \frac{f\left(t-\frac{r}{c_\mathrm{f}}\right)}{r} + \frac{g\left(t+\frac{r}{c_\mathrm{f}}\right)}{r}, \tag{17}$$

in which the solution is represented as the sum of two radial waves, one divergent and the other convergent. The convergent wave is incompatible with the boundary conditions of the free field. In a closed cavity the reflection and so the convergent wave is described by the wall boundary conditions. Therefore, the convergent contribution of the spherical wave can be neglected in the monopole description. Moreover, the sound pressure decays with the distance.

Finally, the solution is transformed in Eq. 17 in the frequency domain:

$$p(r,\omega) = A(\omega)\frac{e^{-ikr}}{r} \tag{18}$$

where A is the monopole amplitude, that depends on ω, and k the wave number. Moreover, the monopole can be defined from its volume velocity $\dot{Q}_s$ and its acoustic power W respectively:

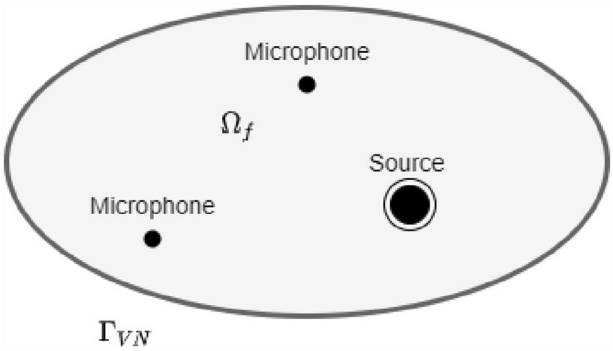

Fig. 1 The 2D sketch of the closed cavity with its elements: the fluid domain Ω_f inside the cavity surrounded by the rigid walls Γ_{VN}, the spherical source and the virtual microphones for the pressure measurement

$$\dot{Q}_s = \frac{4\pi A}{i\omega\rho_f} \tag{19}$$

$$W = \frac{\rho_\mathrm{f} c_\mathrm{f} k^2 \dot{Q}_\mathrm{s}^2}{8\pi}, \tag{20}$$

In the finite element model the monopole is described as an imposed pressure on a node, which represents the centre of the sphere. In Actran the monopole is similarly described, between our formulation and commercial software's one there is a factor in the pressure equal to 4π.

4 FEM Model

4.1 Box Cavity

The generic closed cavity system is sketched in Fig. 1 and it is composed by the closed cavity (the fluid and the Von Neumann boundary condition), the source (or sources) and by the virtual microphones (field points), which are the points where the pressure is calculated.

The first geometrical model is a closed cavity $0.75 \times 0.40 \times 0.65$ m filled by air ($\rho = 1.225\,\mathrm{kg/m^3}$ and $c = 340$ m/s) or water ($\rho = 997\,\mathrm{kg/m^3}$ and $c = 1500$ m/s) and modeled with $15 \times 8 \times 13$ Hexa8 elements with linear interpolation, see Fig. 2a. Two different configurations are selected for the validation:

- only one monopole placed in a corner of the cavity (0.05, 0.05, 0.05 m) with a baseline amplitude of 1 N/m;
- three monopoles placed in three different positions (0.05, 0.05, 0.05 m; 0.55, 0.25, 0.15 m; 0.15, 0.15, 0.50 m) with a fixed amplitude equal to 1 N/m for the first two monopoles and equal to 2 N/m for the last.

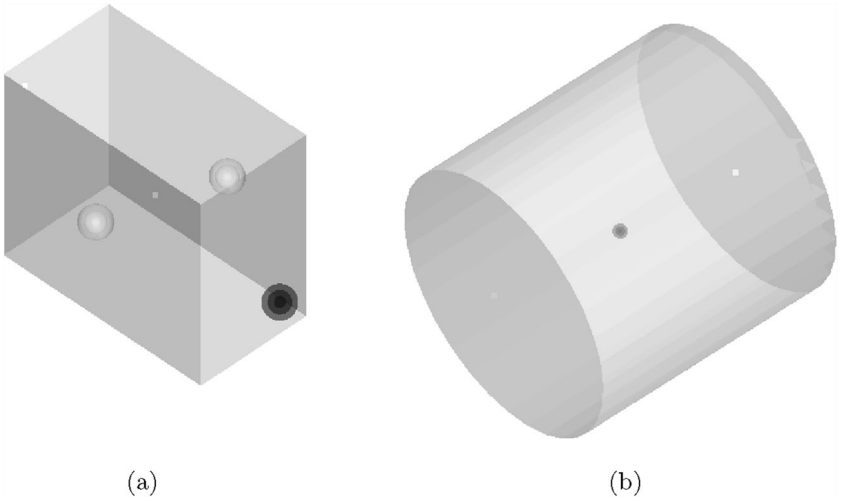

Fig. 2 The two cavity models with the sources (spheres) and the microphones (white points). **a** The box cavity (in black the sphere for the first cases and in white the spheres added in the last case). **b** The cylindrical cavity

In the cavity, the pressure is calculated in two points $A = (0.71, 0.36, 0.61)$ m and $B = (0.375, 0.200, 0.325)$ m.

The elements size h is chosen in order to capture the problem minimum wavelength $\lambda_{\min}$:

$$\lambda_{\min} = \frac{c_{\mathrm{f}}}{f_{\max}}, \tag{21}$$

where $f_{\max}$ is the maximum frequency of the problem, for our problem 1000 Hz, and so the minimum wave length is equal to 0.34 m. The elements size is equal to 0.05 m. The elements are 6.8 times smaller than the smallest wavelength. Actran suggests having an element size around 6–7 times smaller than the minimum wavelength for a linear interpolation. Moreover, according to the works by Marburg [29] and Langer et al. [30], more than six elements per wavelength they are enough to solve the problem. This is also confirmed by the comparison with the analytical solution in Sect. 4.3. The degrees of freedom (DoF) of the model are 2016 with one DoF for each node (the pressure in Eq. 6).

A deeper description of the configurations is reported in Sect. 5.

4.2 Cylindrical Cavity

The cylindrical closed cavity has a length of 0.2 m and a radius of 0.1 m, see Fig. 2b. The elements are Hexa8 (20 on the length and 18 on the diameter) with linear interpolation. The cavity is filled with air and a monopole is placed at the centre of the cylinder. The amplitude is equal to 1 N/m. In the cavity the pressure is calculated in two points $A = (0.010, 0.014, 0.133)$ m and $B = (0.069, 0.072, 0.175)$ m. The medium elements size criterion is fully satisfied with more than 10 elements per wavelength.

4.3 Cavity Validation

MUL2 has already been validated for acoustic computations in [20] by the authors themselves, where the natural frequencies of a cubic cavity were calculated. For the avoidance of doubt, the eigenfrequencies of the box cavity are estimated, both with MUL2 and Actran, and compared to the analytical ones. The natural frequencies f_{ijm} for a box cavity depend on its geometry and on the fluid:

$$f_{ijm} = \frac{c_{\mathrm{f}}}{2} \cdot \sqrt{\left(\frac{i}{a}\right)^2 + \left(\frac{j}{b}\right)^2 + \left(\frac{m}{c}\right)^2},$$

in which a, b and c are the three geometrical dimensions of the cavity, c_f the fluid's speed of sound, i, j and k are the modal order along the three axes. Table 1 reports the calculated modes and their relative errors between the numerical solutions and the analytical one in terms of natural frequencies. The errors between the analytical solution and the numerical one are below the 1% and between the two software are negligible.

For the cylindrical cavity there is not an analytical solution for a completely closed cavity. Although, there is an analytical solution for a cylinder with open surfaces at the two bases [31]. This solution can be applied to our closed cavity only for pure symmetrical longitudinal modes defined by the positive integer n and so it is possible to simplify the equation in [31]:

$$f_n = \frac{c_{\mathrm{f}} n}{2L}, \tag{22}$$

in which L is the cylinder length.

Therefore, the Actran and the MUL2 results are compared. For the longitudinal modes, the numerical results are validated by the analytical solution, as reported in Table 2. The relative errors in terms of natural frequencies

Table 1 The first ten natural frequencies [Hz] calculated by the analytical method, by MUL2 and by Actran with their relative errors and differences between the two software for a rectangular cavity [20]

Modes	Types	Analytical [Hz]	MUL2 [Hz]	Actran [Hz]	MUL2 error [%]	Actran error [%]	MUL2 vs Actran[%]
1	Axial	226.67	227.08	227.08	1.83E–01	1.83E–01	2.81E–06
2	Axial	261.54	262.18	262.18	2.44E–01	2.44E–01	2.72E–06
3	Tangential	346.09	346.85	346.85	2.17E–01	2.18E–01	2.88E–06
4	Axial	425.00	427.74	427.74	6.44E–01	6.44E–01	2.77E–06
5	Axial	453.33	456.65	456.65	7.33E–01	7.33E–01	2.74E–06
6	Tangential	481.67	484.28	484.28	5.42E–01	5.42E–01	2.70E–06
7	Tangntial	499.03	501.69	501.69	5.34E–01	5.34E–01	2.75E–06
8	Axial	523.08	526.56	526.56	6.67E–01	6.67E–01	2.86E–06
9	Tangential	532.34	528.18	528.18	7.80E–01	7.80E–01	2.74E–06
10	Oblique	548.09	550.69	550.69	4.74E–01	4.74E–01	2.83E-06

In the last case, the differences begin from the fifth decimal place

Table 2 The first ten natural frequencies [Hz] calculated by the analytical method only for the longitudinal modes, by MUL2 and by Actran with their relative errors and differences between the two software for a cylindrical cavity [31]

Modes	Analytical [Hz]	MUL2 [Hz]	Actran [Hz]	MUL2 error [%]	Actran error [%]	MUL2 vs Actran [%]
1	850.00	850.87	850.87	1.03E–01	1.03E–01	2.78E–06
2		1001.40	1001.27			1.28E–02
3		1001.44	1001.32			1.22E–02
4		1314.07	1313.98			7.42E–03
5		1314.11	1314.01			7.11E–03
6		1663.49	1664.82			8.04E–02
7		1669.43	1667.70			1.04E–01
8	1700.00	1707.00	1707.00	4.12E–01	4.12E–01	2.69E–06
9		1868.47	1869.66			6.37E–02
10		1873.77	1872.22			8.24E–02

are negligible again. Although, there are two coexistent modes around 1000 Hz, so the frequency maximum limit of the analysis of cylindrical cavity is increased from 1000 to 1100 Hz in order to capture these two modes and to compare the results.

5 MUL2 Validation

In order to validate the monopole source in MUL2 the following analyses are performed:

- direct frequency analyses for a closed box with a spherical source inside and filled by air. The source has a variable amplitude from 0.01 to 100 N/m. The aim is to understand if the spherical source implemented in MUL2 works for a wide range of amplitudes (and so of intensities);
- direct frequency analysis for a closed box with a spherical source inside and filled by water. The aim is to validate the source for a denser material. The amplitude is fixed;
- direct frequency analysis for a closed box with three spherical sources inside and filled by air. MUL2 has to correctly and automatically describe the interactions between the several spherical sources. The monopoles' amplitudes are fixed;
- direct frequency analysis for a closed cylinder with a spherical source inside and filled by air. The aim is to explore the source behaviour in a fuselage-like cavity. The amplitude of the monopole is fixed.

The selected frequency range is from 5 to 1000 Hz (to 1100 Hz for the cylinder) with a step of 1 Hz, so in the low and the mid frequency range. FEM methods in vibroacoustic are usually limited to the low frequency range, in particular for complex models, as an aircraft fuselage. In fact, if there is an increase in the maximum frequency of the problem, according to Eq. 21, the minimum wavelength will decrease and so the model needs smaller

Table 3 The percentage gap in terms of maximum, average and standard deviation between the two software for all the analysed configurations

Cavity	Fluid	Monopole(s) amplitude [*N/m*]	Field point *A* [%]			Field point *B* [%]		
			Δ_{max}	Δ_{av}	Δ_{SD}	Δ_{max}	Δ_{av}	Δ_{SD}
Box	Air	0.01	1.25E–01	1.03E–03	2.59E-02	1.23E-01	3.31E-04	1.62E-02
Box	Air	0.1	1.25E–01	1.03E–03	2.59E–02	1.23E–01	3.31E–04	1.62E-02
Box	Air	0.5	1.25E–01	1.03E–03	2.59E–02	1.23E–01	3.31E–04	1.62E-02
Box	Air	1	1.25E–01	1.03E–03	2.59E–02	1.23E–01	3.31E–04	1.62E-02
Box	Air	10	1.25E–01	1.03E–03	2.59E–02	1.23E–01	3.31E–04	1.62E-02
Box	Air	100	1.25E–01	1.03E–03	2.59E–02	1.23E–01	3.31E–04	1.62E-02
Box	Water	1	1.51E–03	1.52E–05	5.03E–06	2.05E–04	6.35E–05	8.55E-08
Box	Air	1, 1, 2	2.98E–01	1.44E–03	1.17E–01	1.22E–01	3.08E–04	1.54E-02
Cylinder	Air	1	3.63E+03	6.70E+00	1.33+07	1.00E+02	3.05E–01	1.23E+04
“	“	“		5.27E–02[3]			5.21E-02[4]	

[3] Error calculated as comparison between the curves areas

[4] Ibid

elements, rising the number of nodes and so the degrees of freedom of the system.

The results are compared in terms of pressure over the frequency. The differences Δ depends on frequency too. The maximum value Δ_{max}, the average value Δ_{av} and the standard deviation Δ_{SD} of the percentage gap for the different cases are calculated and compared on the two field points.

Finally, to evaluate the improvement of a Layer Wise model in a vibro-acoustic analysis, a coupled analysis is performed in order to solve the plate-cavity problem. The high reliability of the CUF compared to the classical Equivalent Single Layer theory has been already demonstrated by the work of Cinefra et al. [20]. The aim is to validate this higher accuracy for the monopole too. The coupled equations are solved in a similar way of the Eq. 12 through the fundamental nuclei formulation [18–20]. The continuous displacements u_i in the CUF formulation are expressed from the nodal displacement U for the $k-th$ layer of the plate:

$$u_i^k(x,\ y,\ z,\ t) = F_\tau^k(z) N_i(x,\ y) U_\tau^k(t), \tag{23}$$

in which N_i are the shape functions and F_τ^k the thickness functions, which rebuild the solution on the thickness and they are based on Lagrange interpolation polynomials. For this model the results are expressed both in terms of pressure and displacements. The plate is simply supported on its four edges. The plate is placed on the whole upper face of the cavity. The plate's thickness is equal to 0.01 m. The monopole amplitude is 1 N/m and it is placed in a corner of the cavity (0.05, 0.05, 0.05 m). The elements of the plate are homogeneous to those of the fluid, so with a size 0.025 m and a quadratic interpolation (Hexa27 and Quad9) in or 1 N/mder to guarantee the accuracy of the analysis according to Marburg [29] and Langer et al. [30]. Two direct frequency analyses are performed with different materials for the plate:

- one layer of aluminum ($E = 7.2\,\text{GPa}$, $\nu = 0.33$, $\rho = 2700\,\text{kg/m}^3$);
- one layer of an orthotropic material (a polymer material used in additive manufacturing with the following properties $E_1 = E_2 = 1.4\,\text{GPa}$, $E_3 = 1.02\,\text{GPa}$, $\nu_{12} = \nu_{23} = \nu_{13} = 0.35$, $G_{23} = G_{13} = 0.5185\,\text{GPa}, G_{12} = 0.3778\,\text{G Pa}, \rho = 1040\,\text{kg/m}^3$ the layer is made of a particular class of orthotropic material: a transversely isotropic material).

The results are calculated in two points. The first one inside the cavity at position $A = (0.51, 0.36, 0.51\ \text{m})$ and the second one in the plate $B = (0.32, 0.19, 0.65\ \text{m})$. Moreover, according to the CUF approach, the isotropic and the orthotropic plates are solved through three points on the thickness (LW3) interpolation with DoF equal to 18,972 (14,259 for the fluid and 4713 for the structure).

6 Results

6.1 Box Cavity

The results are reported in Table 3. The differences between the two software are caused by the different formulation. Although, these deviations are very small, below 0.1% for the pressure in Pascal. In Fig. 3 the pressure in point A and B for the 1 N/m amplitude monopole and a box filled by air are reported. The discrepancies are constant with the

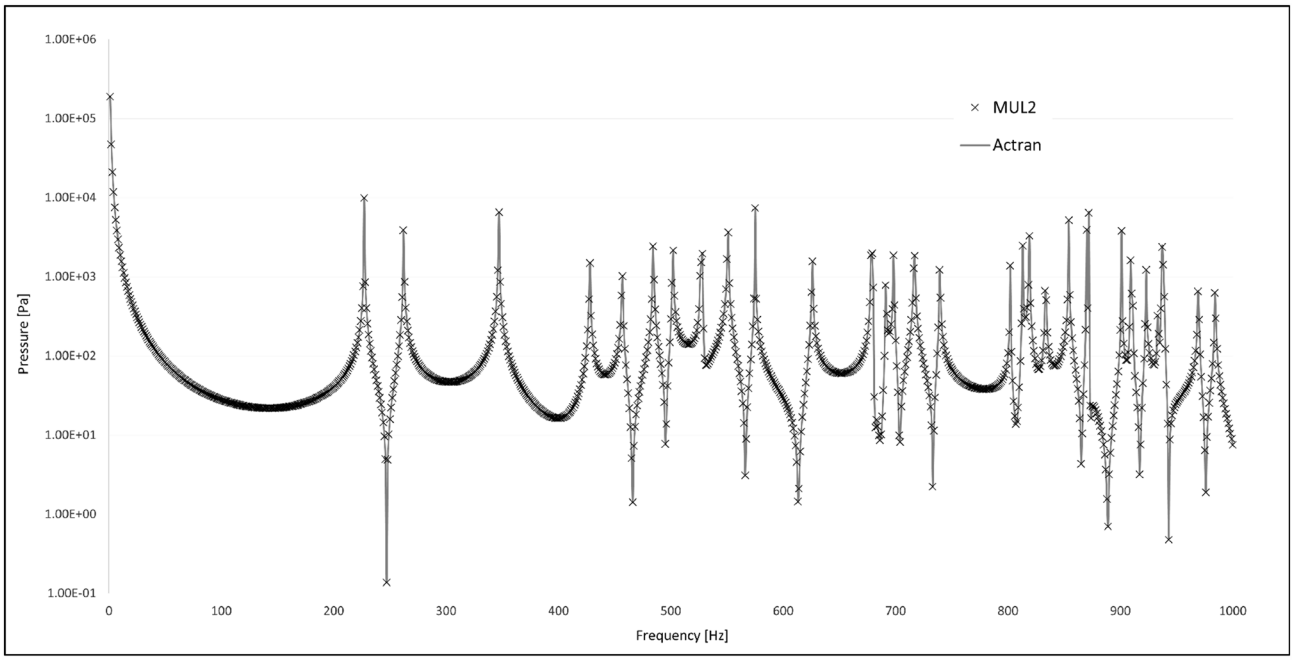

(a)

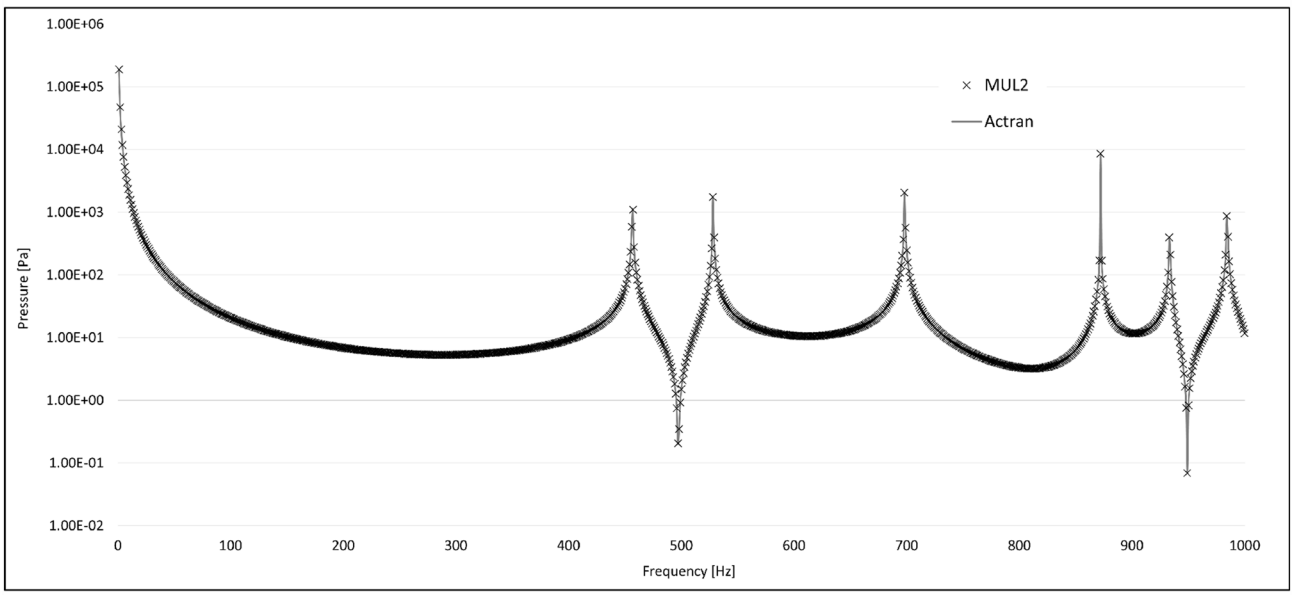

(b)

Fig. 3 The pressure [Pa] in a logarithmic scale for the box cavity with a monopole of 1 N/m amplitude. The results of MUL2 are compared to those by Actran. Although, because the values of the gap are quite small with respect to the pressure absolute values, the curves seem to be overlapped. **a** Point A. **b** Point B

amplitude of the monopole. On the contrary, the differences between MUL2 and Actran decrease changing the fluid material: from air to water (Figs. 4 and 5a). So the differences are caused by the two FEM formulations. Probably in the mass matrix it could be found the reason of this gap. In fact, increasing the sound of speed of the material and so decreasing the factor $1/c_f^2$, that pre-multiplies the mass matrix, the differences between the two software decrease. Therefore, MUL2 new source is able to completely describe the monopole behaviour and the results are very similar to those obtained by Actran, except for a negligible difference caused by the different formulation and the numerical unavoidable small errors. Moreover, if the pressure is converted

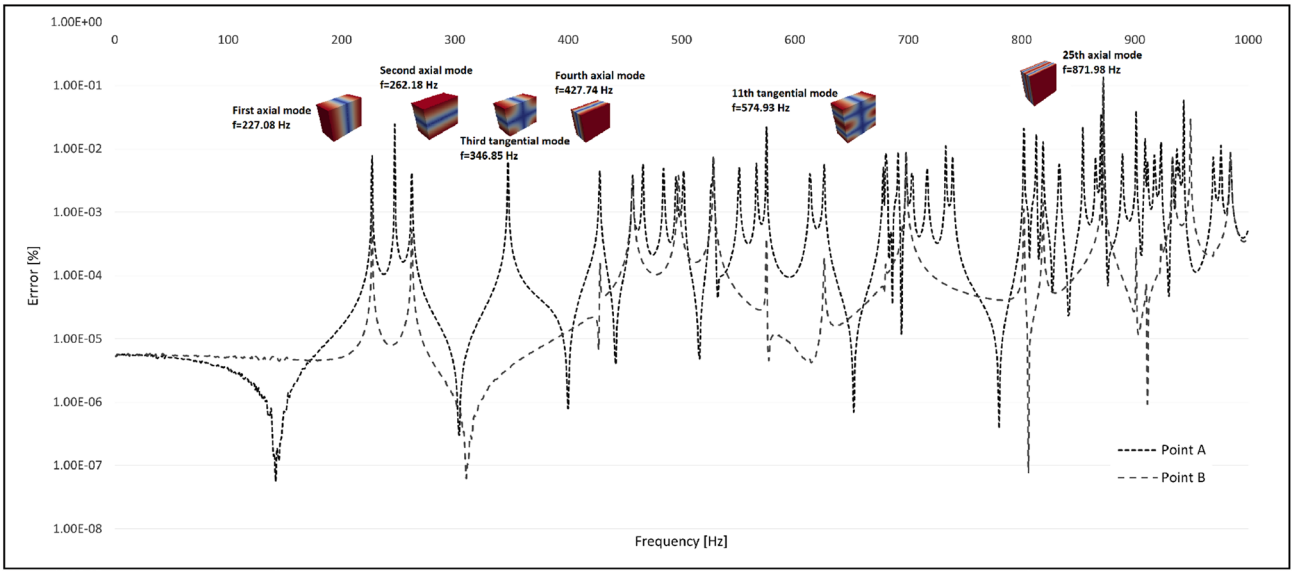

Fig. 4 The gap [%] in a logarithmic scale between MUL2 and Actran for the two field points in the baseline case of one monopole of amplitude equal to 1 N/m in box cavity. The peaks of the differences correspond to the natural frequency of the system (peak in the pressure value) and deep in the pressure value, so where there is an important increase in the pressure derivative

from Pascal to Decibel the error will further decrease, caused by the logarithmic scale of dB, defined as:

$$\mathrm{SPL} = 10 \times \log_{10}\left(\frac{p}{p_{\mathrm{ref}}}\right)^2 \tag{24}$$

in which *SPL* is the sound pressure level in dB, p the pressure in Pascal and $p_{\mathrm{ref}} = 20\,\mu\mathrm{Pa}$ the reference pressure.

MUL2 shows a good accuracy with several monopoles too, Fig. 5b. So, it is able without any modification to describe the interaction between several spherical sources with different amplitudes and so intensities. The presence of several sources shadows the differences in the matrix formulation.

In general, for all the cases, the maximums in differences between MUL2 and Actran are located in correspondence of peaks and deeps of the pressure-frequency curve. The linear regression of the gap increases with the frequency (Fig. 4). So, at low frequency there is the highest accuracy. The maximum gap is located for the axial mode at 872 Hz where there is the absolute peak of pressure.

6.2 Cylinder

The results of the cylindrical cavity between the two models are comparable along almost the whole frequency range. Although, there is a difference near the peaks and deeps, this difference is caused by a difference in the value of the pressure. The peaks are shifted of few Hertz, and this create an important local error, even if the pressure responses are very similar. This local difference strongly affects the average gap between the two software and the maximum, these results are reported in Table 3, while the gap curve is reported in Fig. 6. Moreover, the pressure responses are reported in Fig. 7. The peak and deep due to the two spinning mode around 1000 Hz are clearly visible in both the responses. In order to better compare the two curves avoiding the influence of the peak shifting the difference between the areas defined by the two curves (so the integral) is calculated through the trapezoidal rule. The final relative difference is equal to 0.052% for both the points.

6.3 Coupled Plate-Cavity System

In the coupled case, the results are estimated both in terms of pressure inside the cavity and of displacements in the plate. The comparisons between Actran and MUL2 are in Fig. 8 for the isotropic plate and in Fig. 9 for the orthotropic one. Both the results show a good convergence between the two software. Although, as the frequency increases, the displacements tend to diverge. According to previous studies [20], the ESL based software is no longer able to correctly interpret the mechanical behaviour of the plate. This tendency is almost negligible in the isotropic material but becomes significant with orthotropic material. These differences seem to not influence the fluid behaviour, probably due to low drawback of fluid-structure coupling.

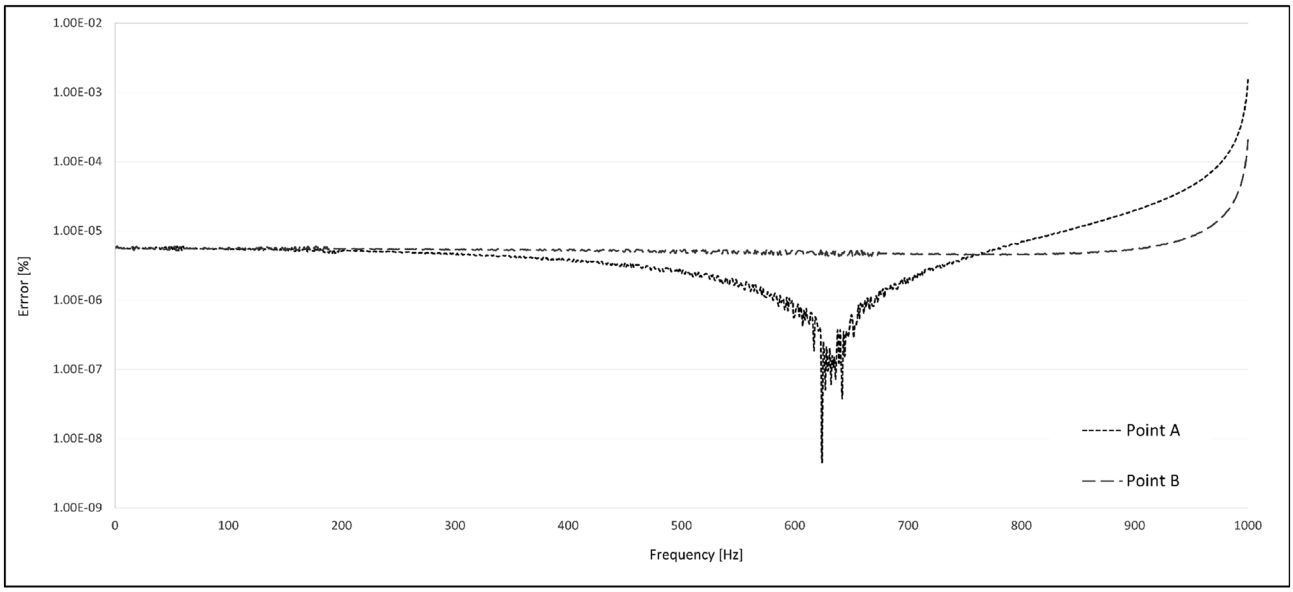

(a)

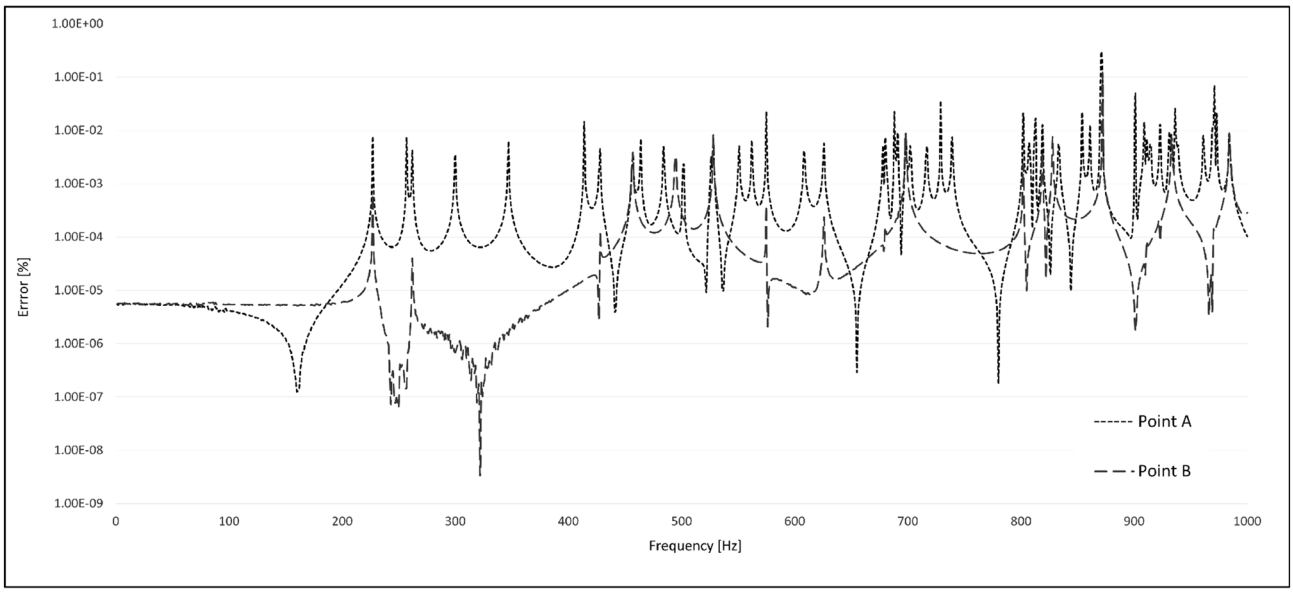

(b)

Fig. 5 The gap [%] in a logarithmic scale between MUL2 and Actran for the two field points in following the cases: **a** one monopole of amplitude equal to 1 N/m in a box cavity filled by water and **b** three monopoles (amplitudes 1 N/m, 1 N/m and 2 N/m) in a box cavity filled by air

7 Conclusions

The validation of the MUL2's monopole with Actran in a closed cavity has been successfully conducted. The medium difference for the box cavity was always below 0.2% and the maximum below 0.3%. Moreover, considering the Decibel scale, due to the logarithmic scale the gaps decrease even more. This gap is probably caused by the different formulation of the fluid elements, so between the classical FEM-ESL formulation of Actran and the CUF of MUL2 with the fundamental nuclei notation. This reason seems to be confirmed by the constant

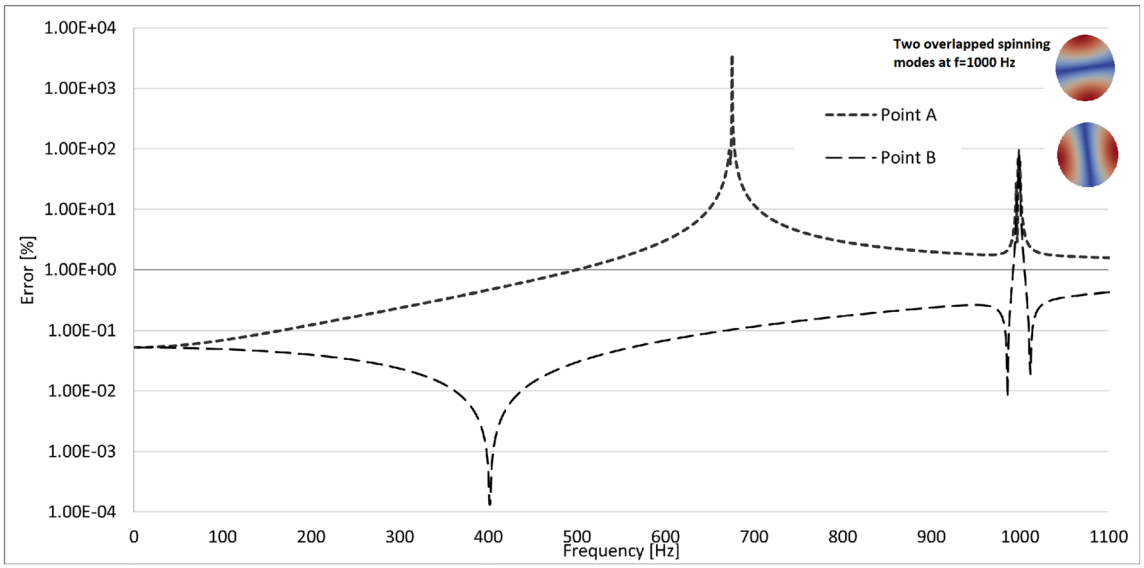

Fig. 6 The gap [%] in a logarithmic scale between MUL2 and Actran for the two field points in the case of one monopole of amplitude equal to 1 N/m in a cylindrical cavity. The peak of the differences corresponds to the natural frequency of the system (peak in the pressure value) and deep in the pressure value, so for the two coexistent spinning modes at 1000 Hz

trend of the error with the monopole amplitude and the decrease of the error rising the density and speed of sound of the fluid (from air to water). The cylindrical cavity presents an acceptable average error 3.5%, the overall frequency responses of the software are comparable to those obtained for the box cavity. Although, the error is strongly affected by the frequency shifting of the pressure response and if the areas of the curves are compared, the total error is reduced to 0.052%, which is more accurate than the simple pressure value comparison for this kind of curves with a very similar trend. Moreover, in the frequency range of the FEM analyses for the aircraft noise problem (around 500 Hz or below [22, 32]), the differences between the two software are much smaller. The average values below 500 Hz for the box cavity will be around 2.5E–04% (max. 0.25E–02%) and 1.5E–01% (max. 9.0E–01%) for the cylinder, with the comparison of the areas the error does not change significantly. As expected, the difference between the two tools increases around the peaks and the deeps of the pressure response, but it still remains low.

The coupled analysis confirms the previous results. The numerical LW approach keeps its advantages in the structural domain in terms of accuracy, due to the CUF, according to [20]. Therefore, the presence of a new acoustic source does not alter the power of the fundamental nuclei formulation. Moreover, it would be possible to more accurately estimate the transmission loss and frequency response of plates stressed by acoustic loads. This was not possible before through the CUF, due to the lack of acoustic loads in its original structural formulation and in the MUL2 library. Until now, the CUF approach was only applied to solve structural and vibro-acoustic problems where the loads were only structural, so the acoustic external loads vector F_p was always equal to zero. In this paper the effectiveness of the CUF is demonstrated with an acoustic load too.

The new implemented source will be exploited in fuselage-like environment and to estimate the frequency response in coupled cavity-plate system with a multi-layers structure, as those exploited by the lining panels of a passenger cabin. Moreover, new acoustic sources and boundary conditions must be implemented in order to expand the choice and power of MUL2: in particular one of the first development will be to implement the infinite elements described by Schroeder [33], similar to a Sommerfeld boundary condition. These elements allow to model the free field boundary condition and so it will be possible to study the monopole behaviour in a free field, of which the analytical solution is known. An imposed pressure (Dirichlet condition), and an impedance (Robin condition) boundary condition, the implementation of plane wave, dipole and quadruple will complete the MUL2 library.

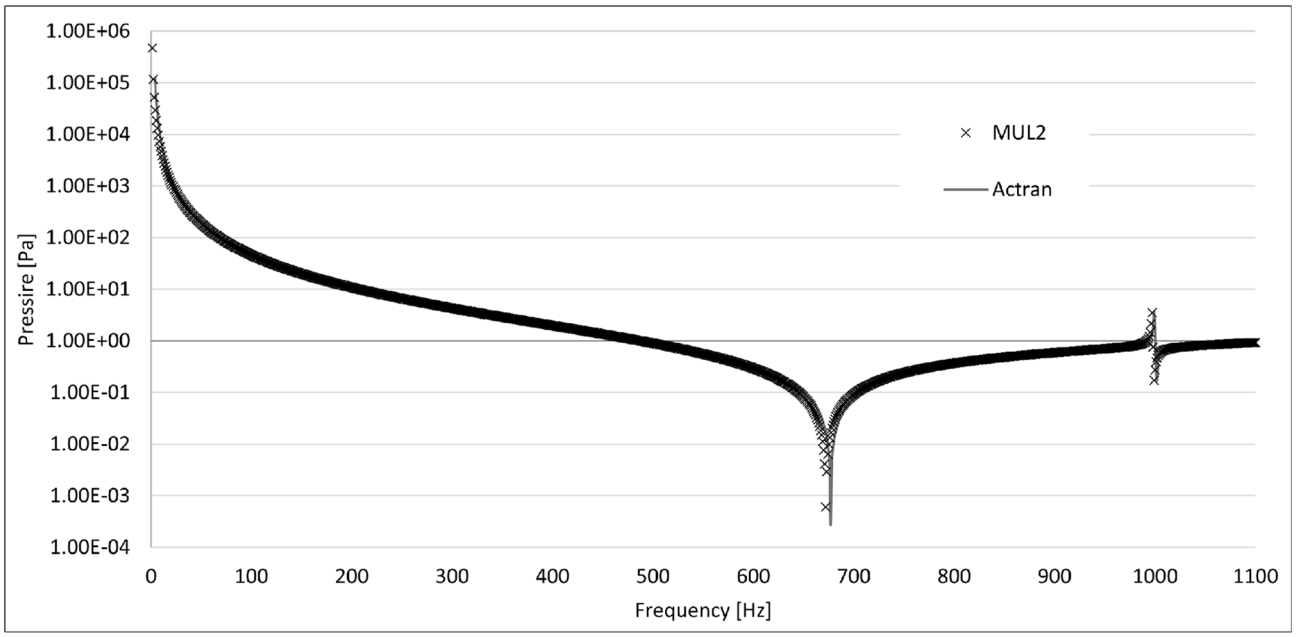

(a)

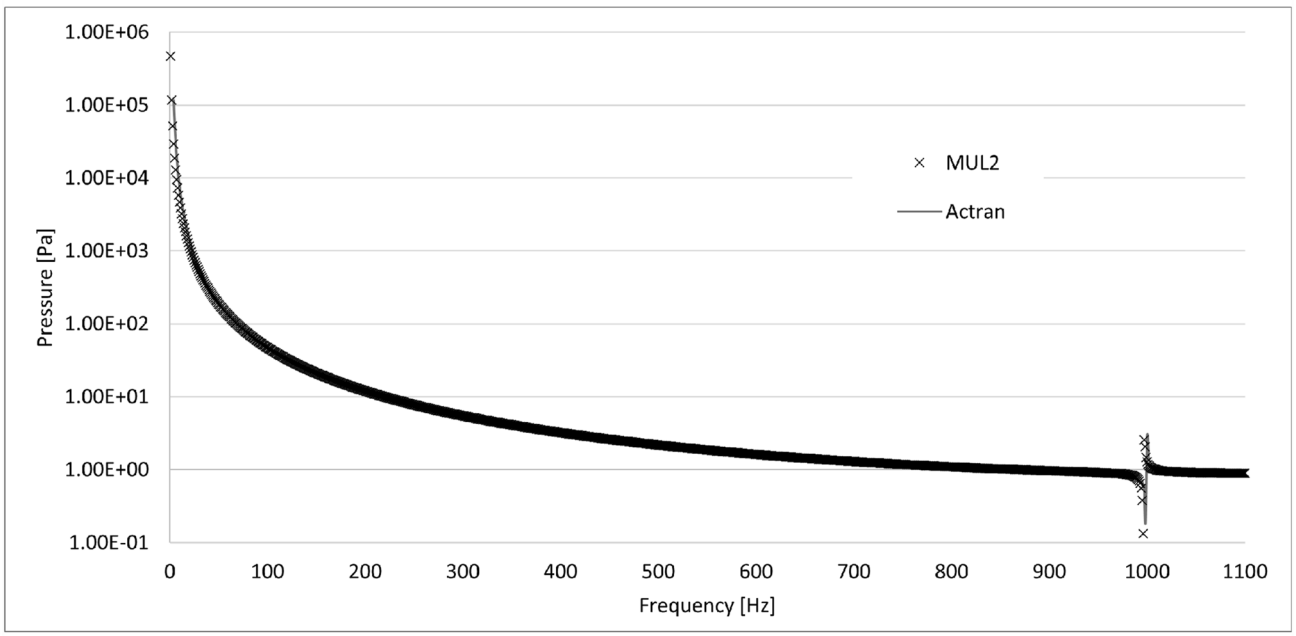

(b)

Fig. 7 The pressure [Pa] in a logarithmic scale for the cylindrical cavity with a monopole of 1 N/m amplitude. The results of MUL2 are compared to those of Actran. **a** Point A. **b** Point B

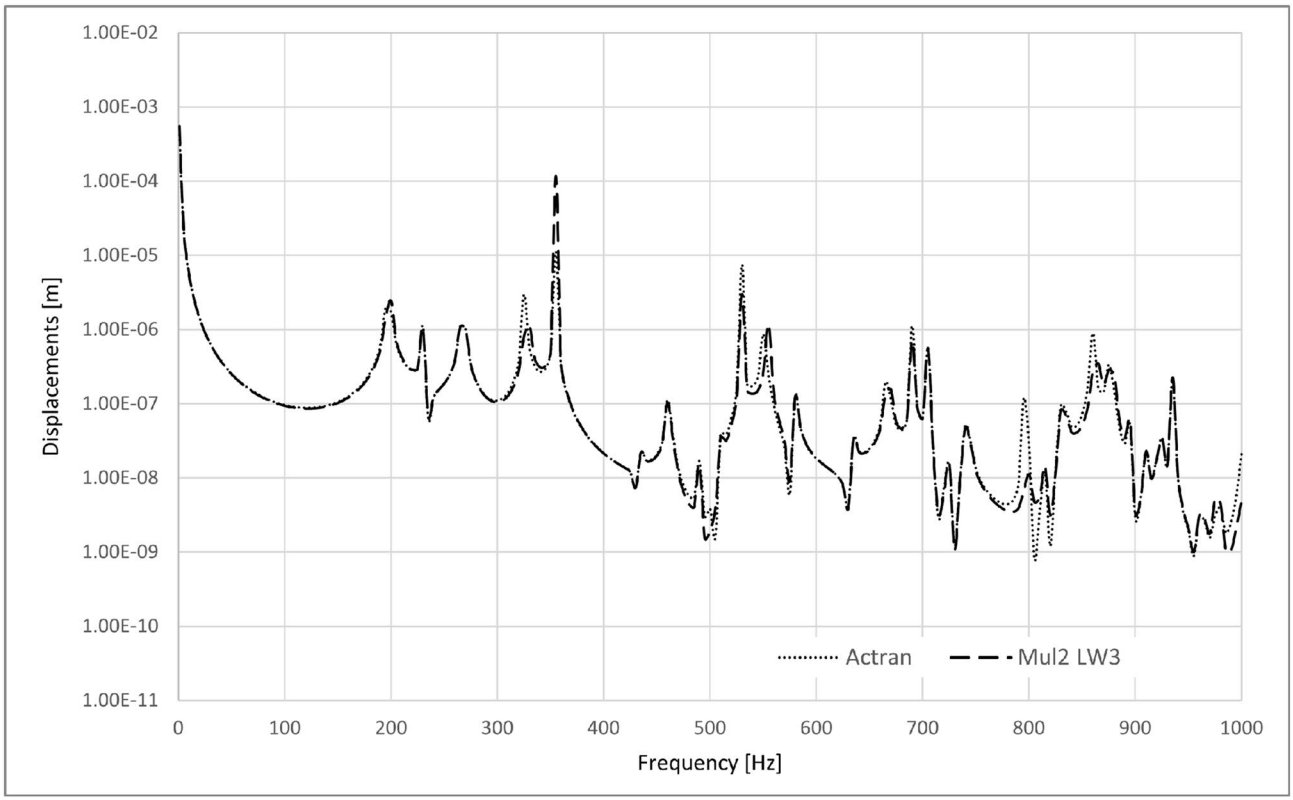

(a)

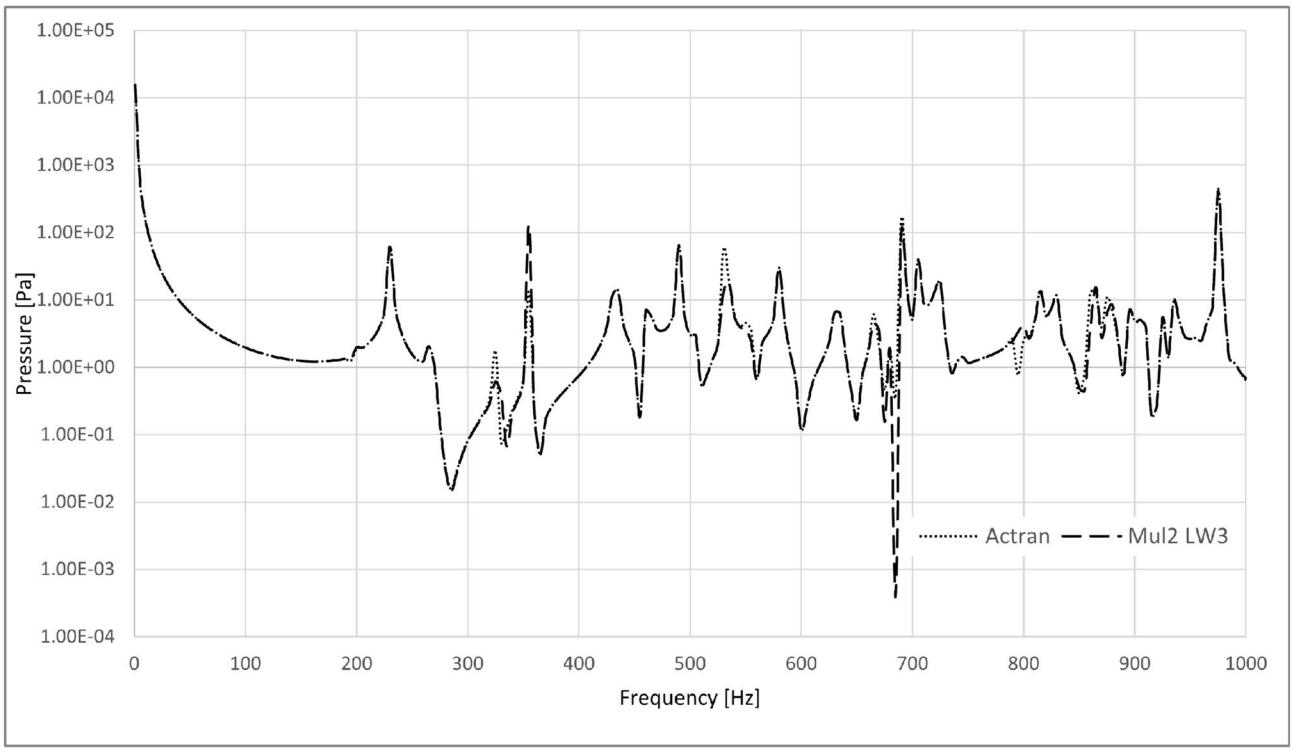

(b)

Fig. 8 The frequency response of the isotropic plate and the coupled cavity calculated by Actran (ESL approach) and MUL2 (LW3 approach). **a** Displacements [m] on the plate at point B. **b** Pressure [Pa] inside the cavity at point A

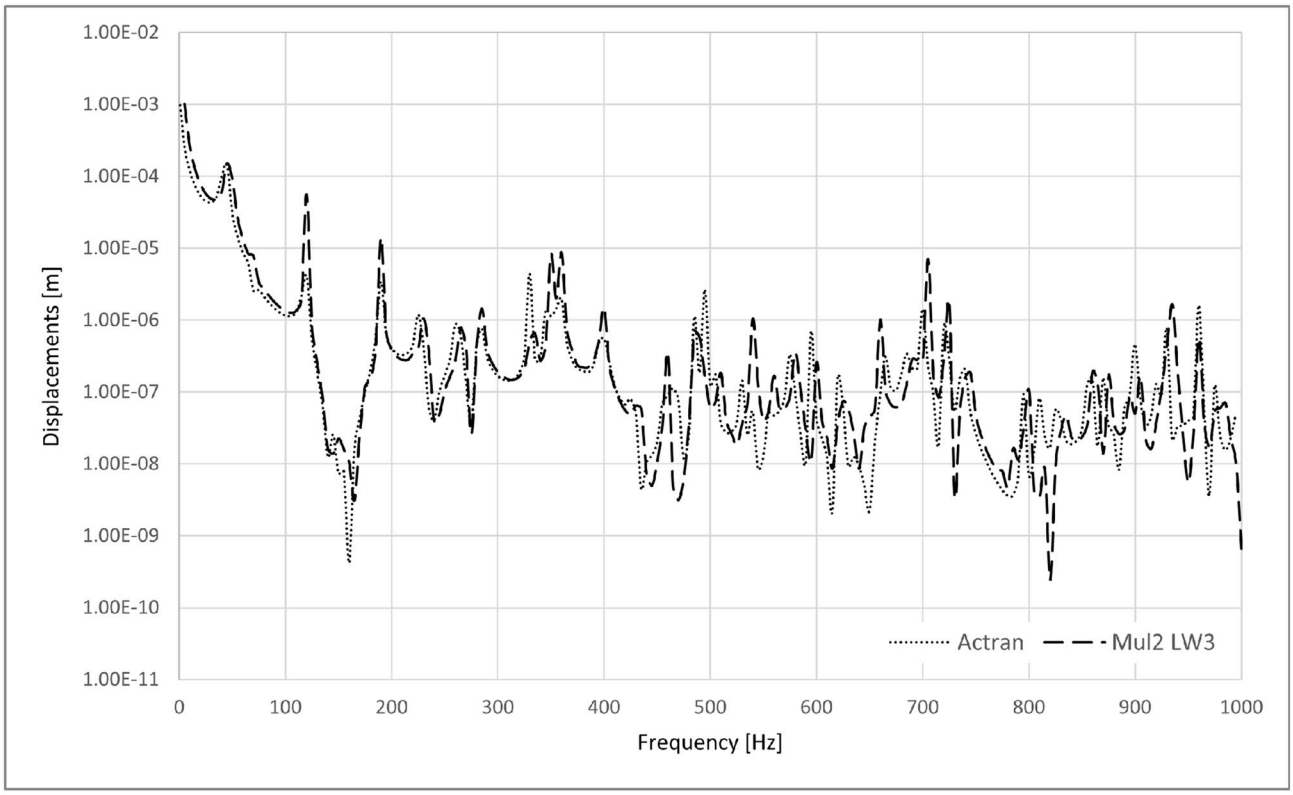

(a)

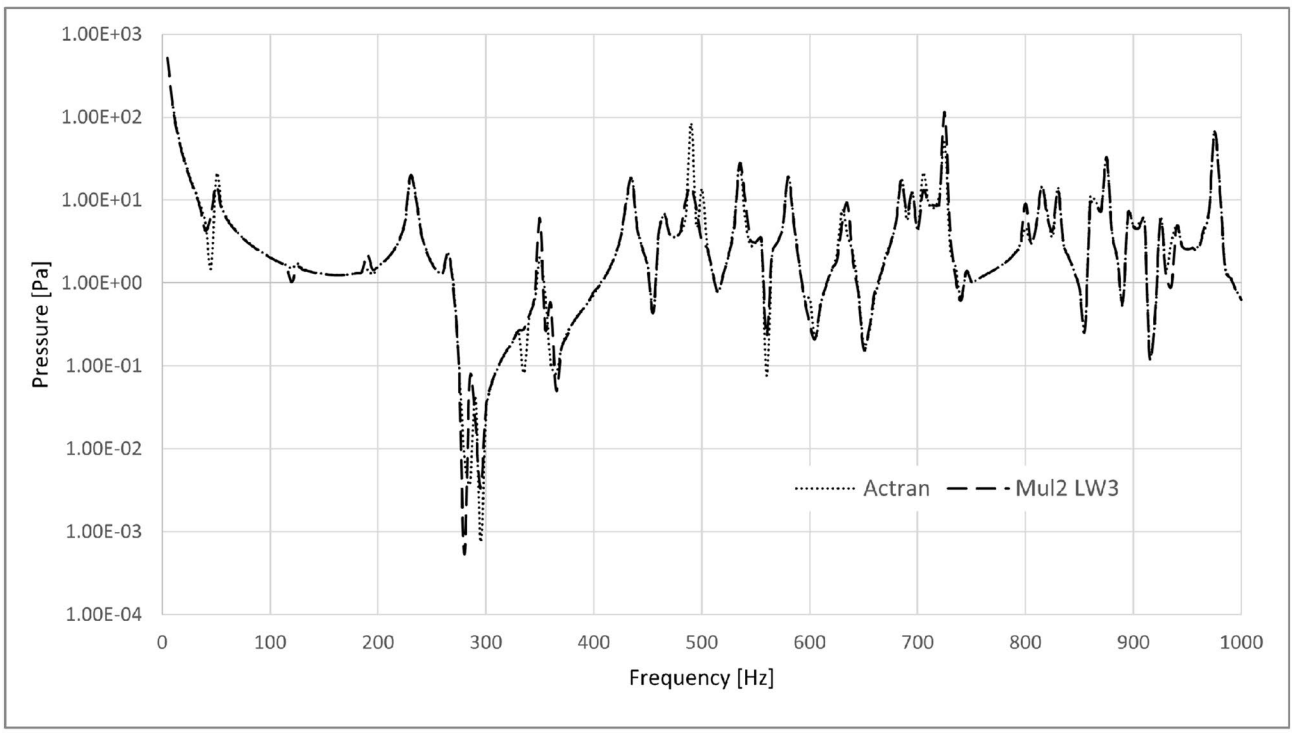

(b)

Fig. 9 The frequency response of the orthotropic plate and the coupled cavity calculated by Actran (ESL approach) and MUL2 (LW3 approach). **a** Displacements [m] on the plate at point B. **b** Pressure [Pa] inside the cavity at point A

Funding Open access funding provided by Alma Mater Studiorum - Università di Bologna within the CRUI-CARE Agreement.

Declarations

Conflict of interest On behalf of all authors, the corresponding author states that there is no conflict of interest.

References

1. Morrell, S., Taylor, R., Lyle, D.: A review of health effects of aircraft noise. Austral. N. Z. J. Public Health **21**(2), 221–236 (1997)
2. Pepper, C., Nascarella, M., Kendall, R.: A review of the effects of aircraft noise on wildlife and humans, current control mechanisms, and the need for further study. Environ. Manag. **32**, 418–32 (2003)
3. Pennig, S., Quehl, J., Rolny, V.: Effects of aircraft cabin noise on passenger comfort. Ergonomics **55**, 1252–65 (2012)
4. Dobrzynski, W.: Almost 40 years of airframe noise research: what did we achieve? J. Aircr. **47**, 353–367 (2010)
5. Marulo, F.: Aircraft community noise: the revenge of a neglected problem. Aerotec Missili Spazio **94**, 184–194 (2015)
6. Bhat, W.V., Wilby, J.F.: Interior noise radiated by an airplane fuselage subjected to turbulent boundary layer excitation and evaluation of noise reduction treatments. J. Sound Vib. **18**(4), 449–464 (1971)
7. Orrenius, U., Cotoni, V., Wareing, A:. Analysis of sound transmission through aircraft fuselages excited by turbulent boundary layer or diffuse acoustic pressure fields. In: 38th International Congress and Exposition on Noise Control Engineering 2009, INTER-NOISE 2009, **4**, 2637–2645, (2009)
8. Casalino, D., Diozzi, F., Sannino, R., Paonessa, A.: Aircraft noise reduction technologies: a bibliographic review. Aerosp. Sci. Technol. **12**(1), 1–17 (2008)
9. Leylekian, L., Lebrun, M., Lempereur, P.: An overview of aircraft noise reduction technologies. Aerospacelab **7**, 1–15 (2014)
10. Rao, M.: Recent applications of viscoelastic damping for noise control in automobiles and commercial airplanes. J. Sound Vib. **262**, 457–474 (2003)
11. Pirk, R., Jonckheere, S., Pluymers, B., Desmet, W.: Vibro-acoustic modeling and validation using viscoelastic material. Compt Rendus Méc **345**(3), 208–220 (2017)
12. Cinefra, M., Passabì, S., Carrera, E.: Fem vibroacoustic analysis in the cabin of a regional turboprop aircraft. Adv Aircr Spacecr Sci **5**, 477–498 (2018)
13. Petrone, G., Melillo, G., Laudiero, A., De Rosa, S.: A statistical energy analysis (sea) model of a fuselage section for the prediction of the internal sound pressure level (spl) at cruise flight conditions. Aerosp. Sci. Technol. **88**, 340–349 (2019)
14. Cotoni, V., Shorter, P., Langley, R.: Numerical and experimental validation of a hybrid finite element-statistical energy analysis method. J. Acoust. Soc. Am. **122**(1), 259–270 (2007)
15. Atalla, N., Bernhard, R.J.: Review of numerical solutions for low-frequency structural-acoustic problems. Appl. Acoust. **43**(3), 271–294 (1994)
16. D'Alessandro, V., Petrone, G., Franco, F., De Rosa, S.: A review of the vibroacoustics of sandwich panels: Models and experiments. J. Sandw. Struct. Mater. **15**(5), 541–582 (2013)
17. Cinefra, M., De Miguel, A.G., Filippi, M., Houriet, C., Pagani, A., Carrera, E.: Homogenization and free-vibration analysis of elastic metamaterial plates by Carrera unified formulation finite elements. Mech. Adv. Mater. Struct. **28**, 1–10 (2019)
18. Carrera, E., Cinefra, M., Petrolo, M., Zappino, E.: Finite Element Analysis of Structures Through Unified Formulation. Wiley, Hoboken, New Jersey, USA (2014)
19. Li, G., Carrera, E., Cinefra, M., De Miguel, A.G., Pagani, A., Zappino, E.: An adaptable refinement approach for shell finite element models based on node-dependent kinematics. Compos. Struct. **210**, 1–19 (2018)
20. Cinefra, M., Moruzzi, M.C., Bagassi, S., Zappino, E., Carrera, E.: Vibro-acoustic analysis of composite plate-cavity systems via cuf finite elements. Compos. Struct. **259**, 113428 (2021)
21. Bertsch, L., Snellen, M., Enghardt, L., Hillenherms, C.: Aircraft noise generation and assessment: executive summary. CEAS Aeronaut. J. **10**, 3–9 (2019)
22. Moruzzi, M.C., Cinefra, M., Bagassi, S.: Vibroacoustic analysis of an innovative windowless cabin with metamaterial trim panels in regional turboprops. Mech. Adv. Mater. Struct. **28**, 1–13 (2019)
23. Trompette, N., Guerich, M.: An experimental validation of vibro-acoustic prediction by the use of simplified methods. Appl. Acoust. **66**(4), 427–445 (2005)
24. Marchetto, C., Maxit, L., Robin, O., Berry, A.: Vibroacoustic response of panels under diffuse acoustic field excitation from sensitivity functions and reciprocity principles. J. Acoust. Soc. Am. **141**(6), 4508–4521 (2017)
25. Vieira, A., Snellen, M., Malgoezar, A.M.N., Merino-Martinez, R., Simons, D.G.: Analysis of shielding of propeller noise using beamforming and predictions. J. Acoust. Soc. Am. **146**(2), 1085–1098 (2019)
26. Moruzzi, M.C., Cinefra, M., Bagassi, S., Carrera, E. Attenuation of noise in the cabin of a regional aircraft by metamaterial trim panels. In: 32th ICAS 2020 Proceedings, pp. 1–11 (2021)
27. Migeot, J.L., Coyette, J.P., Grègory, L. Acoustics, pp. 101–105. IJK Numerics, Bruxelles, Belgium (2016)
28. Kinsler, L.E., Frey, A.R., Coppens, A.B., Sanders, J.V.: Fundamentals of Acoustics, pp. 127–130. Wiley, Hoboken, New Jersey, USA (2000)
29. Marburg, S.: Six boundary elements per wavelength: is that enough? J. Comput. Acoust. **10**(01), 25–51 (2002)
30. Langer, P., Maeder, M., Guist, C., Krause, M., Marburg, S.: More than six elements per wavelength: The practical use of structural finite element models and their accuracy in comparison with experimental results. J. Comput. Acoust. **25**(04), 1750025 (2017)
31. Rona, A.: The acoustic resonance of rectangular and cylindrical cavities. J. Algorithms Comput. Technol. **1**(3), 329–356 (2007)
32. Hesse, C.: Active control of composite fuselage type structures with enclosed acoustic cavity. J. Fluids Struct. **81**, 565–573 (2018)
33. Schroeder, E.A.: Infinite elements for three-dimensional fluid-structure interaction problems. DTRC-87/047, (1987)